The International Society of Precision Agriculture presents the
15th International Conference on Precision Agriculture
26–29 JUNE 2022
Minneapolis Marriott City Center | Minneapolis, Minnesota USA

Potential of UAS Multispectral Imagery for Predicting Yield Determining Physiological Parameters of Cotton

Amrit Pokhrel[1], Simerjeet Virk[1], John L. Snider[1], George Vellidis[1], and Ved Parkash[1]

[1] Department of Crop and Soil Sciences, University of Georgia Tifton Campus, 2360 Rainwater Road, Tifton, GA, 31793, USA.

A paper from the Proceedings of the
15th International Conference on Precision Agriculture
June 26-29, 2022
Minneapolis, Minnesota, United States

Abstract.

The use of unmanned aerial systems (UAS) in precision agriculture has increased rapidly due to the availability of reliable, low-cost, and high-resolution sensors as well as advanced image processing software. Lint yield in cotton is the product of three physiological parameters: photosynthetically active radiation intercepted by canopy (IPAR), the efficiency of converting intercepted active radiation to biomass (RUE), and the ratio of economic yield to total dry matter (HI). The relationships between lint yield and vegetation indices (VI's) in cotton have been extensively studied; however, reports addressing the yield determining physiological parameters are far less common. A study was conducted during the 2021 growing season with the objective of relating different VI's derived from UAS multispectral imagery with yield-determining physiological parameters (IPAR, RUE, and HI) of cotton. Five different nitrogen treatments were applied to generate substantial variability in canopy development and yield. Multispectral imagery was collected fortnightly along with light interception and biomass measurements throughout the season. Several different VI's were computed using the red (668 nm), blue (475 nm), green (560 nm), near-infrared (842 nm), and red-edge (717 nm) spectral bands. A regression analysis was performed to identify VI's that can be used to predict IPAR, biomass, and RUE in cotton. Data analysis indicated that power functions best described the relationship of IPAR and cotton biomass with VI's. GNDVI and SCCCI explained more than 90% of variation in IPAR with R^2 value of 0.929 and 0.906, respectively. Similarly, cotton biomass was found to be strongly related with RVI (R^2 = 0.932) and NDRE (R^2 = 0.916). In context of RUE, most of the variation was best explained by GRVI (linear relationship with R^2 0.549) and GNDVI (linear relationship with R^2 0.419). The results from this study show that VI's such as GNDVI, RVI, and GRVI derived from UAS multispectral imagery could potentially be used to predict certain physiological parameters (IPAR, biomass, and RUE) of cotton within a growing season. Utilizing UAS technology to predict

these parameters can help in advancing high throughput phenotyping and prediction of yield driving parameters in response to nitrogen.

Keywords.
Unmanned Aerial System, Multispectral imagery, Cotton, Physiological parameters, Yield prediction, Vegetation Indices.

Introduction

Remote sensing has gradually evolved from low-resolution orbital satellite imagery to utilization of advanced, high-resolution unmanned aerial systems (UAS) in recent years. The availability of reliable, low-cost, and high-resolution sensors as well as advanced and automated image processing software have increased the application of UAS in crop phenotyping and agricultural management (Barnes et al., 1996; Schuckman & Dutton, 2017). Unmanned aerial vehicles configured with multispectral sensors capture reflected spectral signature, within the spectral wavelength range from 475 nm to 842 nm, that can be used to define important crop characteristics like canopy cover, biomass as well as detection of stress symptoms.

In the field of precision agriculture, UAS can assist in real-time crop information collection and further utilizing that information for in-season crop management decisions (Stafford, 2000; Warren and Metternicht, 2005). UAS imagery has been used for mapping field variability and soil properties, crop species classification, growth monitoring, phenotyping, stress detection, yield prediction, etc. (Ballester et al., 2019; Gutierrez et al., 2012; Xu et al., 2019). Also, UAS has very wide compatibility for different vegetations and crops as it can be used in forestry, turf grasses, berries, grapes, and especially row crops like cotton.

Cotton has global importance as a commercial crop with high export value and substantial contribution to the global clothing and textile industry (Sui et al., 2017). The United States (US) is one of the top three cotton producing countries with yield forecasted around 18.3 million bales in 2021. The US is also a prime exporter of cotton with around 35% of global cotton exports (USDA, 2021). Out of all cotton producing states in the US, Georgia comes at the second place in terms of cotton harvested area of 1.2 million acres with production of 2.2 million bales for the cropping year of 2020 (USDA and NAS, 2021).

Cotton possesses unique growth dynamics, such as indeterminate growth and sympodial branching, which makes it a challenging task to predict and manage efficiently. The fact that it is grown as an annual crop despite being a perennial requires extensive crop management for efficient yield production (Mauney, 1986; Sui et al., 2017). According to Monteith (1972), yield is the function of cumulative intercepted photosynthetically active radiation (IPAR) during the growing season, the efficiency with which the crop converts the radiation into biomass (RUE) and the fraction of total biomass allocated to the economically important part of the crop (HI).

$$\text{Yield} = \text{IPAR} \times \text{RUE} \times \text{HI} \quad (1)$$

Out of the several applications of UAS in precision agriculture, yield prediction is one of the areas that needs more exploration. Cotton yield estimation during its growing season can provide producers an early opportunity to manage their limiting inputs to attain profitable yield as well as the knowledge of cotton yield variability in the field makes both defoliation and harvesting process efficient (Huang et al., 2013; Tedesco-Oliveira et al., 2020). There are extensive studies that have related lint yield with derived vegetation indices from multispectral imagery; however, studies relating vegetation indices with yield determining physiological parameters are limited. Therefore, the main objective of this study was to relate yield determining physiological parameters to vegetation indices derived from UAS multispectral imagery.

Materials and Methods

Experimental Layout

A study was conducted at the Lang-Rigdon Farm Station of the University of Georgia Tifton Campus during the growing season of 2021 using Deltapine (DP) 1646 cotton cultivar. The study plots were 6 rows wide by 15 m long, arranged in a completely randomized block design with five different nitrogen application treatments (0, 44, 89, 134, and 179 kg N ha^{-1}) and each treatment replicated 5 times within the field. The different nitrogen application rates were applied to create significant variability in crop growth and yield. All other crop management practices, beside nitrogen treatments, were performed according to the Georgia Cotton Production Guide 2021

(Hand et al., 2021).

Measurements

In-season Data Collection

Above canopy (PARabove) and below canopy (PARbelow) light intensities, and dry weight samples were collected fortnightly throughout the season. Light intensities were measured using AccuPAR LP-80 Ceptometer (Meter Environment, Pullman, WA). For dry weight measurements, above ground biomass samples were collected from 1 m^2 area, followed by oven drying at 80^o C for 48 hours or until constant weight was obtained. There were total 5 sampling times for the growing season of 2021 at 43, 56, 69, 93, and 115 days after planting (DAP). These in-season measurements were further used to calculate two physiological parameters – intercepted photosynthetically active radiation (IPAR) and radiation use efficiency (RUE). The formula to calculate these physiological parameters are shown below:

$$\text{Fraction of IPAR } (IPAR_f) = (PARabove - PARbelow)/PAR\ above \quad (2)$$

$$\text{Total IPAR } (IPAR)\ (MJ\ m^{-2}) = \text{Total Cumulative PAR} * IPAR_f \quad (3)$$

$$RUE\ (g\ MJ^{-1}) = \text{Dry Weight } (g\ m^{-2})/IPAR\ (MJ\ m^{-2}) \quad (4)$$

where, total cumulative PAR = 46% of total solar radiation

UAV Imagery Collection

Both RGB and Multispectral imagery were acquired at each sampling period from the altitude of 45 m. The images were acquired on the same sampling periods as for the physiological measurements i.e. 43, 56, 69, 93, and 115 DAP. The RGB images were acquired using a DJI PHANTOM™ Pro 4 V2.0 (Shenzhen, China) system with an inbuilt visual camera and multispectral imagery was acquired using MicaSense RedEdge-MX™ (Seattle, WA) sensor mounted on a DJI INSPIRE™ 2 (Shenzhen, China) platform. For georeferencing, ground control points (GCPs) were collected using a handheld Trimble GNSS Unit (Sunnyvale, CA) with RTK correction enabled.

Table 1. Technical specifications of camera sensors used for imagery collection.

Technical specification	DJI's PHANTOM™ Pro 4 V2.0	MicaSense RedEdge-MX™
Sensor	1-inch CMOS; 20 Megapixel	RedEdge-MX sensor
Bits per pixel	16 bits	12 bits
Spectral Range	RGB combined	Blue (475 nm), Green (560 nm), Red (668 nm), Red edge (717 nm), near-IR (842 nm)
Ground Resolution	1.33 cm per pixel	3.29cm per pixel per band
Image Overlap	Side 70% Front 80%	Side 80% Front 80%
Flight altitude	45 m	45 m

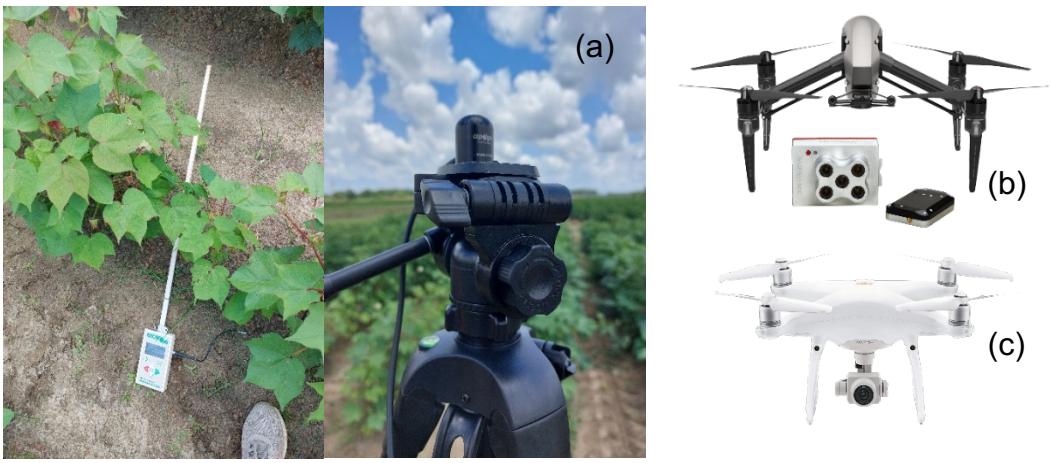

Fig 1. Instruments used for the measurement of physiological parameters and collection of aerial imagery. (a) AccuPAR LP-80 Ceptometer used for collection of below and above canopy light intensities, (b) DJI INSPIRE™ 2 UAV with MicaSense RedEdge-MX™ sensor (c)DJI PHANTOM™ 4 Pro V2.0 with visual sensor.

Image Processing

The Pix4Dmapper® software (Pix4D, Switzerland) was used to process images and create orthomosaic imagery. Radiometric calibration was done for the multispectral imagery using a calibrated reflectance panel recommended for MicaSense RedEdge-MX™. GCPs were also used while processing the images for each acquisition date to georeferenced stitched orthomosaic imagery.

Image Analysis

After image processing, further extraction of the reflectance values for each band of multispectral raster image from the center two rows (ROI) was done in ArcMap® 10.7.1 (ESRI, Redlands, CA). The methodology used in ArcMap is illustrated in the steps below:

1. Classification of aerial raster image for separation of soil and cotton plant was done using multiplication of two indices- Excessive Greeness (ExG) and Normalized Difference Vegetation Index (NDVI); Classification Index: ExG*NDVI
   ExG = 2*Green – Red – Blue (5)
   NDVI = (NIR-Red) / (NIR +Red) (6)

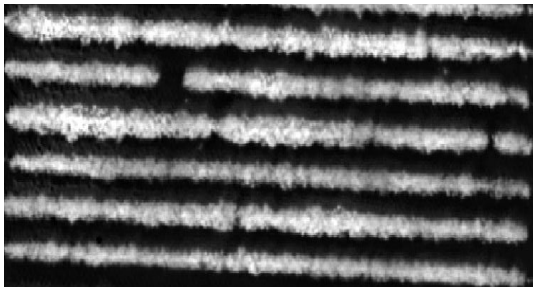

Fig 2. Example of classified aerial image for soil and cotton plant using ExG*NDVI

2. Visual imagery was used to lay out the plots for data extraction and cross check the effectiveness of soil and plant classification.

Fig 3. Example of Visual (RGB) imagery

3. Binary soil mask raster layer was created by determining the threshold value for ExG*NDVI that separates soil and plant. This mask layer was crosschecked with visual imagery.

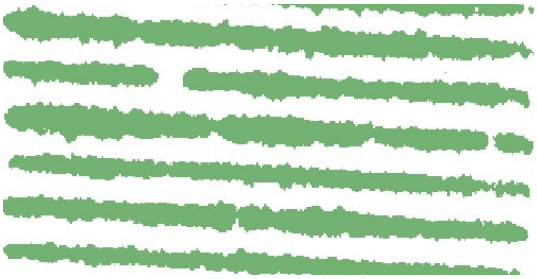

Fig 4. Example of binary mask layer for soil and cotton plant

4. Finally, soil removed reflection indices for all multispectral bands was created using the binary mask layer. Further, reflectance indices values for all 5 bands were extracted from the center two rows (ROI) enclosed by the red line.

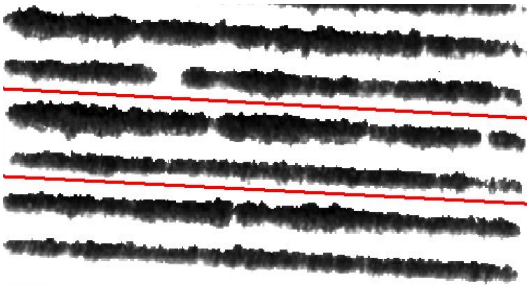

Fig 5. Example of soil removed raster layer and region of interest (ROI)

Vegetation Indices (VI's)

Twenty different vegetation indices (Appendix-Table 2) were identified from available literature related to cotton growth, management and lint yield prediction and calculated from the extracted values for reflectance bands in Microsoft Excel® (Redmond, WA).

Statistical Analysis

Regression analysis was performed to determine the relation of VI's with yield determining physiological parameters and identify VI's that can be used to predict them. Scatterplots for VI's vs IPAR, biomass, and RUE were created for observing coefficient of determination and comparison among the VI's and physiological parameters. Based on the scatterplots, the power function best described the relationship of VI's with IPAR and biomass, which were determined using equation 7.

$$y = ax^b \quad (7)$$

For curve fitting, the power function was converted to simplified linear logarithmic form with natural log-transformed y and x, as shown in equation 8.

$$\ln(y) = \ln(a) + \ln(x) \quad (8)$$

where, y = IPAR (MJ m^{-2}) or biomass (g m^{-2}), and x is the value of VI's.

However, the relationship between VI's and RUE was explained by a simple linear regression, as in equation (9).

$$y = bx + a \quad (9)$$

where, y = RUE (g MJ^{-1}), and x is the value of VI's.

All statistical analysis was performed in JMP® Pro 16 (SAS Institute, Cary, NC) while graphs were created using SigmaPlot 14.0 (Systat Software Inc., San Jose, CA).

Results

IPAR and Biomass related with VI's

IPAR and biomass both showed a power function relationship with VI's; to simplify, the power function (equation 7) was natural log transformed to linear form (equation 8). Out of the 20 VI's, the top 6 VI's, that explained more than 88% variation in both IPAR and Biomass, are shown in the scatterplots in Fig 6 and Fig 7.

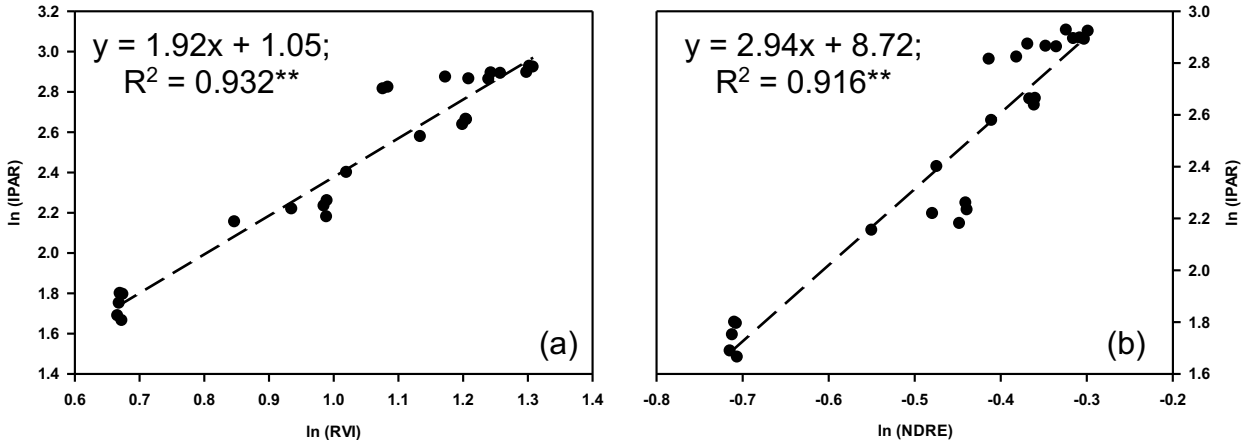

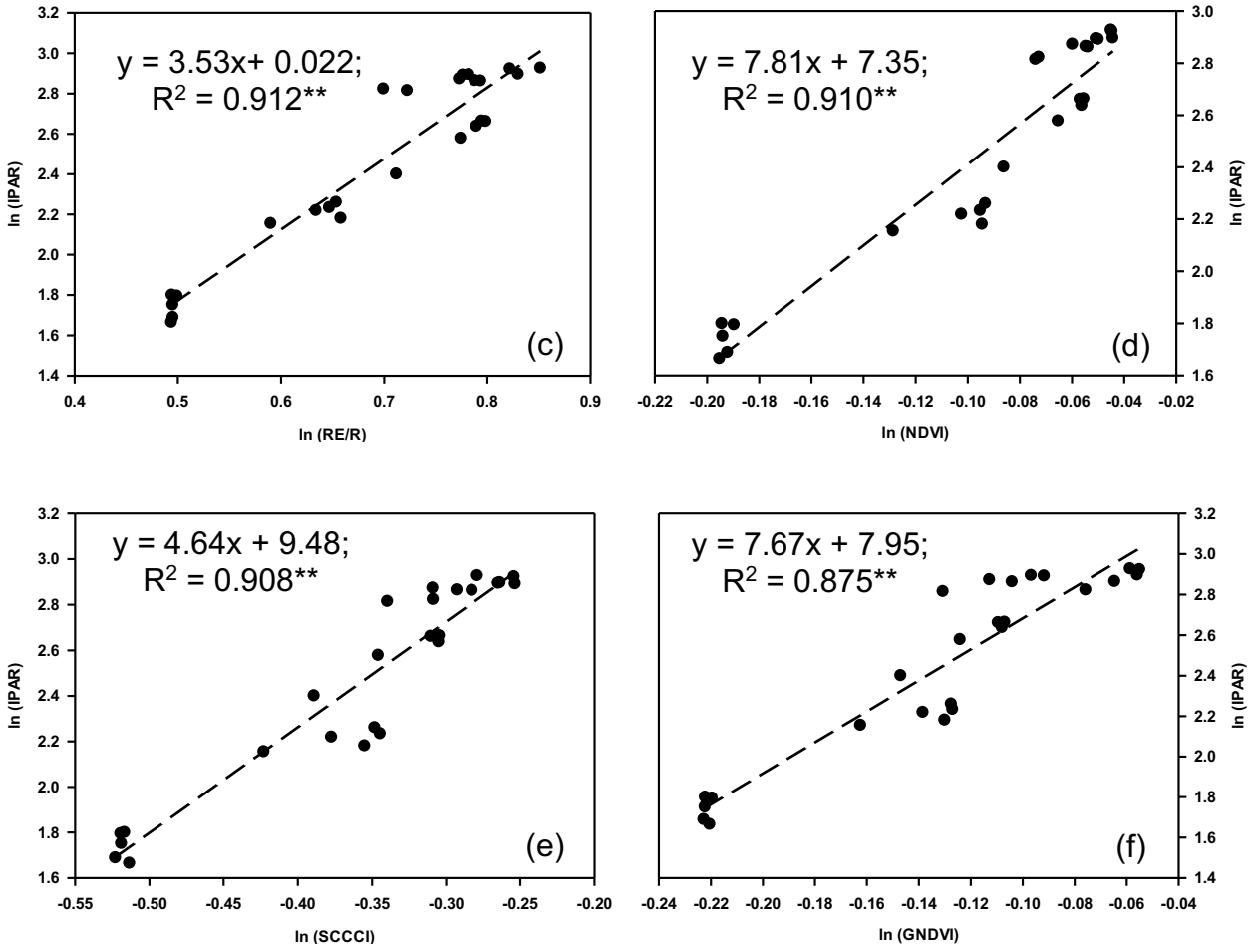

Fig 6. Graphs showing the relationship between different VI's and IPAR. The y axis represents the log-transformed IPAR and x axis represents the log-transformed VI's. ** represents the significance probability level of 0.01.

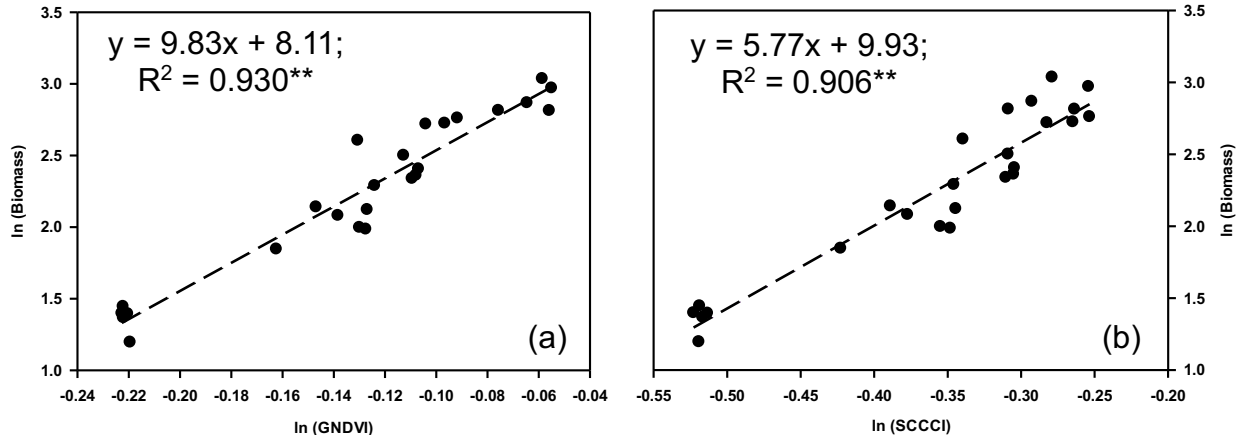

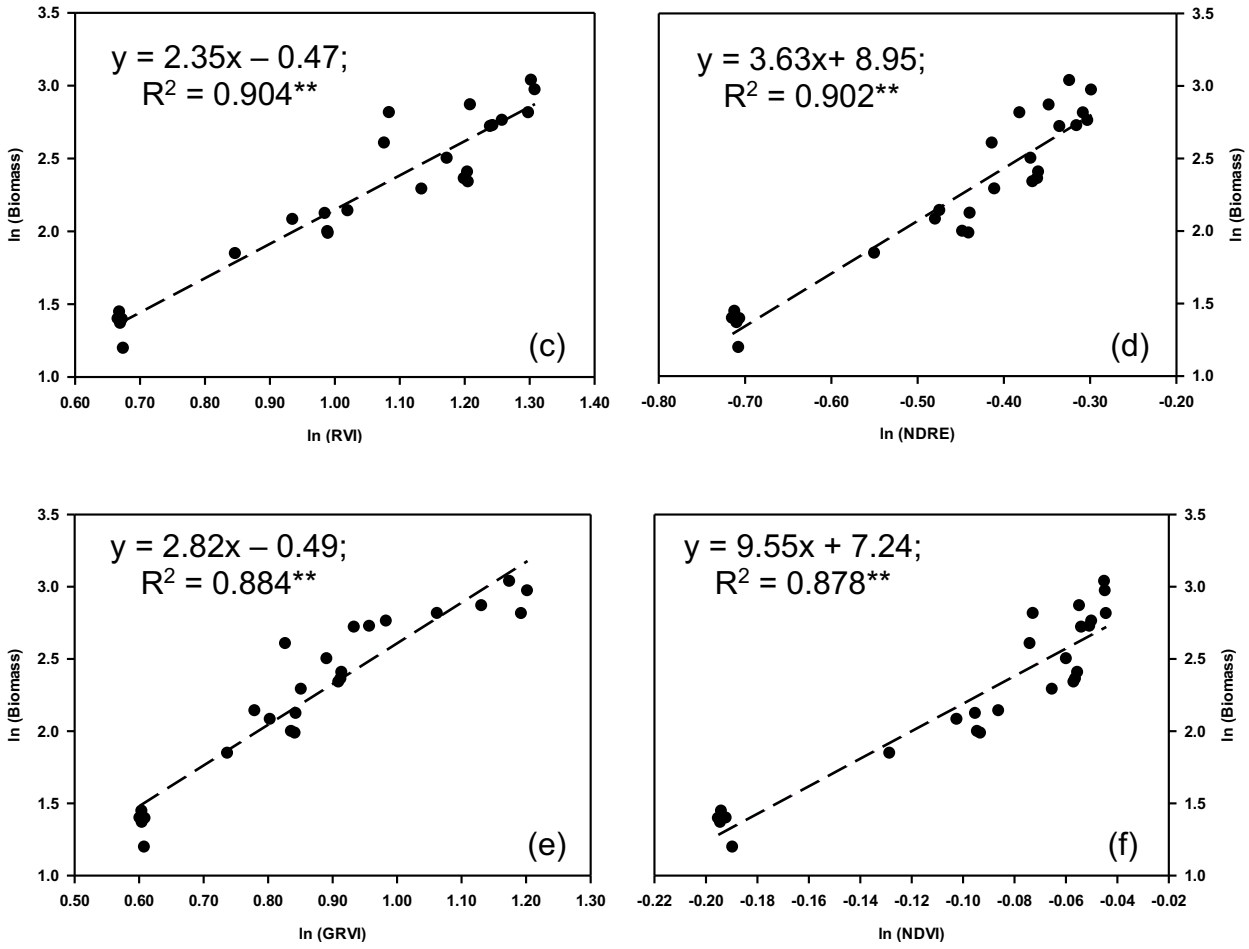

Fig 7. Graphs representing the relationship between different VI's and biomass. The y axis represents the log-transformed biomass and x axis represents the log-transformed VI's. ** represents the significance probability level of 0.01.

The Ratio Vegetation Index (RVI) explained 93.2% of variation in IPAR followed by Normalized Difference Red-edge Index (NDRE) (R^2 = 0.916), Red-edge to Red ratio (RE/R) (R^2 = 0.912), and Normalized Difference Vegetation Index (NDVI) (R^2 = 0.910). Similarly, Green Normalized Difference Vegetation Index (GNDVI) predicted biomass with coefficient of determination value of 0.93, followed by Simplified Canopy Chlorophyll Content Index (SCCCI) (R^2 = 0.906), RVI (R^2 = 0.904), and NDRE (R^2 = 0.902).

RUE correlation with with VI's

Out of total 20, only two VI's showed simple linear relationship with RUE explaining more than 41% of variation (Fig 8). Green Ratio Vegetation Index (GRVI) showed a moderate correlation (R^2 = 0.549) with RUE followed by GNDVI (R^2 = 0.419).

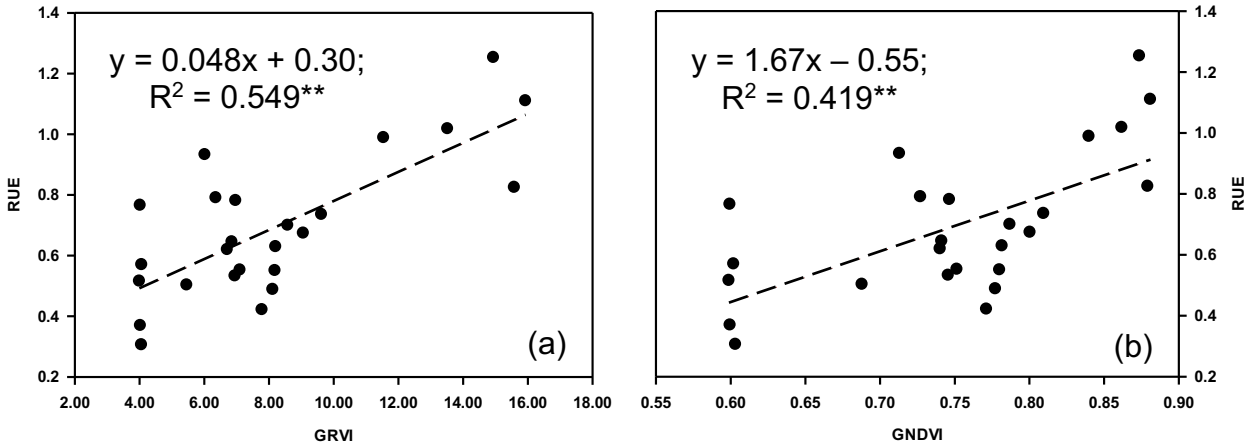

Fig 8: RUE correlation with GRVI and GNDVI. Simple linear regression best explained the relationship between RUE and VI's. The y axis represents RUE and x axis represents VI's. ** represents the significance probability level of 0.01.

Derived RUE and Observed RUE

The two best related VI's with IPAR and biomass were used to derive predicted IPAR and predicted biomass. As we know, biomass is the product of IPAR and RUE. This relationship was used to compute derived RUE using predicted IPAR and predicted biomass.

$$\text{Derived RUE} = \text{Predicted Biomass} / \text{Predicted IPAR} \quad (10)$$

The scatterplots showed that derived RUE with GNDVI (as predictor of biomass) and RVI (as predictor of IPAR) was related to observed RUE with highest R^2 value of 0.598; however, this relationship would not be accurate due to observed clustering of data points in the scatterplot. Therefore, derived RUE with GNDVI (as predictor of biomass) and NDRE (as a predictor of IPAR) was the best relationship which explained 44.4% of variation for observed RUE (Fig 9).

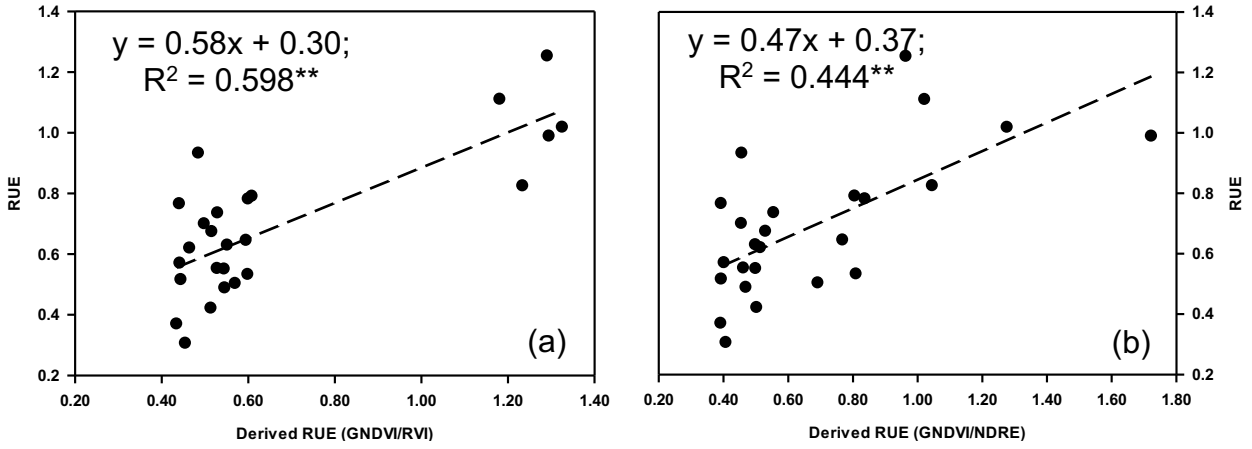

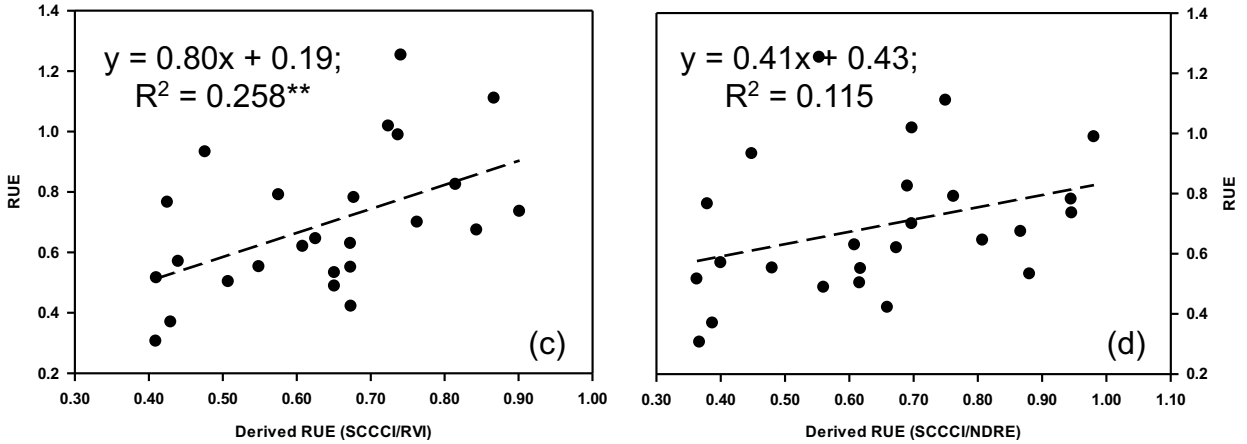

Fig 9. Scatterplots of observed RUE vs derived RUE. Simple linear regression best explained the relationship. The y axis represents observed RUE and x axis represents derived RUE. The indices in parenthesis are the indices used to get predicted biomass and predicted IPAR respectively. ** represents the significance probability level of 0.01.

Summary

In conclusion, VI's derived from multispectral imagery could potentially be used to predict IPAR, biomass, and RUE. Analysis of first-year data of this study showed that the relationship between IPAR, biomass, and VI's can be best explained by power relationships with RVI and NDRE as the predictor of IPAR, and GNDVI and SCCCI as the predictor of biomass. Among the VI's studied, only two VI's, GRVI and GNDVI were linearly related with RUE. Both of these VI's are computed using green and near-infrared spectral bands. These particular bands of light, near infrared and green, are reflected by plants, whereas red and blue spectral bands are absorbed for photosynthesis. This may indicate that the reflectance of green and near-infrared can be related to RUE of cotton canopy. Also, derived RUE using GNDVI and NDRE, as predictor of biomass and IPAR respectively, explained nearly half of the variation in RUE. Findings of this study indicate that multispectral imagery and VI's can be used to predict yield determining physiological parameters like IPAR and RUE of cotton.

Future work aims to determine the VI's that highly correlates with cotton harvest index. If all the cotton physiological parameters can be predicted using multispectral imagery, derivation of a yield prediction model for cotton will be explored further. Future research in 2022 and further will include validation of the yield prediction models as well as improvements to data collection and modelling approaches.

Acknowledgements

The authors would like to thank the Cotton Incorporated, the Georgia Cotton Commission, Lola Sexton, Will Vance, Coleman Byers and Cotton Physiology lab members of UGA Tifton Campus.

References

Ballester, Brinkhoff, Quayle, & Hornbuckle. (2019). Monitoring the Effects of Water Stress in Cotton using the Green Red Vegetation Index and Red Edge Ratio. *Remote Sensing*, *11*(7). https://doi.org/10.3390/rs11070873

Barnes, E. M., Moran, M. S., Pinter Jr, P. J., & Clarke, T. R. (1996). Multispectral remote sensing and site-specific agriculture: Examples of current technology and future possibilities. *Proceedings of the Third International Conference on Precision Agriculture*, 845–854.

Gutierrez, M., Norton, R., Thorp, K. R., & Wang, G. (2012). Association of Spectral Reflectance Indices with Plant Growth and Lint Yield in Upland Cotton. *Crop Science*, *52*(2), 849–857. https://doi.org/10.2135/cropsci2011.04.0222

Hand, C., Culpepper, S., Harris, G., Kemerait, B., Liu, Y., Perry, C., Porter, W., Roberts, P., Smith, A., & Virk, S. (2021). *2021 Georgia Cotton Production Guide*.

Huang, Y. B., Sui, R. X., Thomson, S. J., & Fisher, D. K. (2013). Estimation of cotton yield with varied irrigation and nitrogen treatments using aerial multispectral imagery. *International Journal of Agricultural and Biological Engineering*, *6*(2), 37–41. https://doi.org/10.3965/j.ijabe.20130602.00?

Mauney, J. R. (1986). Vegetative Growth and development of fruiting sites. In J. R. Mauney & J. M. Stewart (Eds.), *Cotton physiology* (Issue 1, pp. 11–28). Cotton Foundation.

Monteith, J. L. (1972). Solar radiation and productivity in tropical ecosystems. *Journal of Applied Ecology*, *9*(3), 747–766.

Schuckman, K., & Dutton, J. (2017). *Multispectral remote sensing systems. Pennsylvania State University, Department of Geography. Basic Concepts of Image Analysis*.

Stafford, J. V. (2000). Implementing precision agriculture in the 21st century. *Journal of Agricultural Engineering Research*, *76*(3), 267–275.

Sui, R., Byler, R. K., & Delhom, C. D. (2017). Effect of nitrogen application rates on yield and quality in irrigated and rainfed cotton. *Journal of Cotton Science*, *21*(2), 113–121.

Tedesco-Oliveira, D., Pereira da Silva, R., Maldonado, W., & Zerbato, C. (2020). Convolutional neural networks in predicting cotton yield from images of commercial fields. *Computers and Electronics in Agriculture*, *171*(February), 105307. https://doi.org/10.1016/j.compag.2020.105307

USDA. (2021). Cotton and Wool Outlook. In *U.S. Department of Agriculture, Economic Research Service*. https://www.ers.usda.gov/webdocs/outlooks/99355/cws-20i.pdf?v=3391.9

USDA, & National Agricultural Statistics Service. (2021). *Crop Production*.

Warren, G., & Metternicht, G. (2005). Agricultural applications of high-resolution digital multispectral imagery. *Photogrammetric Engineering & Remote Sensing*, *71*(5), 595–602.

Xu, R., Li, C., & Paterson, A. H. (2019). Multispectral imaging and unmanned aerial systems for cotton plant phenotyping. *PLoS ONE*, *14*(2), e0205083. https://doi.org/10.1371/journal.pone.0205083

Appendix

Table 2. List of 20 different VI's derived from multispectral imagery in this study.

Abbreviated VI's	Nomenclature	Formula
ExG	Excessive Greenness	$2 \times G - R - B$
NDVI	Normalized Difference Vegetation Index	$\frac{NIR - R}{NIR + R}$
ExG*NDVI	ExG multiplied by NDVI (Classification Index)	$(2 \times G - R - B)\left(\frac{NIR - R}{NIR + R}\right)$
GNDVI	Green Normalized Difference Vegetation Index	$\frac{NIR - G}{NIR + G}$
NDRE	Normalized Difference Red Edge Index	$\frac{NIR - RE}{NIR + RE}$
RVI	Ratio Vegetation Index	$\frac{NIR}{R}$
SCCCI	Simplified Canopy Chlorophyll Content Index	$\frac{NDRE}{NDVI}$
RE/R	Red edge and Red Ratio	$\frac{RE}{R}$
GRVI	Green Ratio Vegetation Index	$\frac{NIR}{G}$
VARI	Visible Atmospherically Resistance Index	$\frac{G - R}{G + R - B}$
TCARI	Transformed Chlorophyll Absorption Reflectance Index	$3\left[(RE - R) - 0.2(RE - G) \times \left(\frac{RE}{R}\right)\right]$
OSAVI	Optimized Soil Adjusted Vegetation Index	$(1 + 1.6)\left(\frac{NIR - R}{NIR + R + 0.16}\right)$
TCARI/OSAVI	TCARI normalized by OSAVI	$\frac{TCARI}{OSAVI}$
SAVI	Soil Adjusted Vegetation Index	$(1 + 0.5)\left(\frac{NIR - R}{NIR + R + 0.5}\right)$
RGBVI	Red Green Blue Vegetation Index	$\frac{G - B \times R}{G^2 + (B \times R)}$
RE/G	Red edge and Green Ratio	$\frac{RE}{G}$
GRedVI	Green Red Vegetation Index	$\frac{G - R}{G + R}$
WDRVI	Wide Dynamic Range Vegetation Index	$\frac{0.2 \times NIR - R}{0.2 \times NIR + R}$
MSAVI2	Modified Soil Adjusted Vegetation Index	$\frac{(2NIR + 1) - \sqrt{(2NIR + 1)^2 - 8(NIR - R)}}{2}$
EVI	Enhanced Vegetation Index	$\frac{2.5 \times NIR - R}{(NIR + 6 \times R - 7.5 \times B) + 1}$